Transient effects on electron spin observation

Article (Published Version)

Transient effects on electron spin observation

J. Larson,[1] B. M. Garraway,[2] and S. Stenholm[1]
[1]*Physics Department, Royal Institute of Technology (KTH), Albanova, Roslagstullsbacken 21, SE-10691 Stockholm, Sweden*
[2]*Department of Physics and Astronomy, University of Sussex, Falmer, Brighton BN1 9QH, United Kingdom*
(Received 18 July 2003; published 12 March 2004)

In an earlier publication we addressed the problem of splitting an electron beam in the Stern-Gerlach experiment. In contrast to arguments put forward in the early days of quantum theory, we concluded that there are no issues of principle preventing the observation of electron spin during free flight. In that paper, however, we considered only a sudden switch off of the separating magnetic field. In this work we consider the possible effects of finite switching times at the beginning and the end of the interaction period. We consider a model where the coupling between the electron and the field is time dependent. As a result of the time dependence, the field also acquires an electric component, but this seems to cause no significant change of our conclusions. On the other hand, the smooth change of the interaction enforces the same longitudinal velocity on the electron both at the beginning and end of the interaction period because of conservation laws; this effect was missing in our earlier calculations. As the electrons are supposed to travel as a beam, this feature helps by restoring the beam quality after the interaction.

DOI: 10.1103/PhysRevA.69.032103 PACS number(s): 03.65.Ta, 03.75.−b, 14.60.Cd, 34.80.Nz

I. INTRODUCTION

In the late 1920s Niels Bohr argued that it was impossible to measure the spin of a free electron using a device such as a Stern-Gerlach magnet. The Bohr argument was based on the Heisenberg uncertainty principle and may be outlined as follows: An electron beam has a finite width resulting in an uncertainty in the Lorentz forces acting on it, due to the variation of the magnetic field across the beam. Because of the size of the electron magnetic moment ($\mu = e\hbar/2m$) it turns out that the uncertainty of the Lorentz forces is of the same order as the spin-splitting force itself. The spin-splitting force arises from the gradient of the field. Thus the two effects are mixed up and an unambiguous measurement of a spin component cannot be made. We have recently reviewed the history of this problem in Ref. [1]. This and other arguments by Mott, Brillouin, and Knauer were put forward by Pauli at one of the Solvay meetings [2]. Bohr was later to argue rather more philosophically about the measurability of electron spin (see, e.g., Ref. [3]), but he stood behind the original argument. We examined this argument in Ref. [4] where we looked in some detail at the dynamics of an electron wave packet in a static inhomogeneous magnetic field. We were able to show that a resolution of electron spin beam components was *just* possible for certain optimum parameters.

A result of *just* resolved spins is the best we have been able to achieve in the conventional transverse Stern-Gerlach beam arrangement. We have, however, noted an improved spin resolution for the longitudinal arrangement in Ref. [4], Sec. VII. This is also the result of Gallup *et al.* [5] in a physically more detailed system. A point of interest has been that the quantum result for spin spitting has been better than the classical result [4–6] if account of the visibility of splitting is taken.

The possibilities and limitations of the typical Stern-Gerlach configuration were debated in the early days of quantum theory. Our earlier publication [4] was mainly aimed at resolving this question. Hence we continue to investigate the transverse problem, where we have focused on a weakness: we did not take into account the effect of the electron entering or exiting the static magnetic field (i.e., the effect of a finite duration of the magnetic field). That is, we considered the electron wave packet to be "born" inside the region of inhomogeneous magnetic field. This might not seem impossible—an electron cathode could well be placed inside a Stern-Gerlach magnetic field, and electron detectors could be inside the field region too. But our analysis in Ref. [4] required an additional free evolution of the electron wave packet *after* leaving the magnetic field.

Thus our purpose here is to look at an electron wave packet encountering and leaving a field region with the aim of measuring a splitting of electron spin components. However, we do *not* do this by considering the propagation of a full three-dimensional (3D) wave packet problem, which is computationally very demanding. Instead we consider a model system where the inhomogeneous magnetic field is turned on, for example, by means of currents in wires, and then, after affecting the motion of the electron wave packet, the magnetic field is turned off. The physical situation might be as represented in Fig. 1. We will focus on the effects of the resulting transients and the finite time necessary for changing the magnetic field.

One main feature of the model is the appearance of the electric field due to the time dependence of the vector potential. This seems not to add any major complications to the treatment. However, one feature which was overlooked in our work [4] was that since the longitudinal momentum component $p_x = mv_x - eA_x$ is conserved in our model, the longitudinal velocity v_x must return to its initial value after the electron has left the field region. This tends to restore the electron beam quality, and is a welcome improvement in the light of making an experimental realization.

We compare our quantum-mechanical result with a classical simulation based on our initial electron ensemble with a

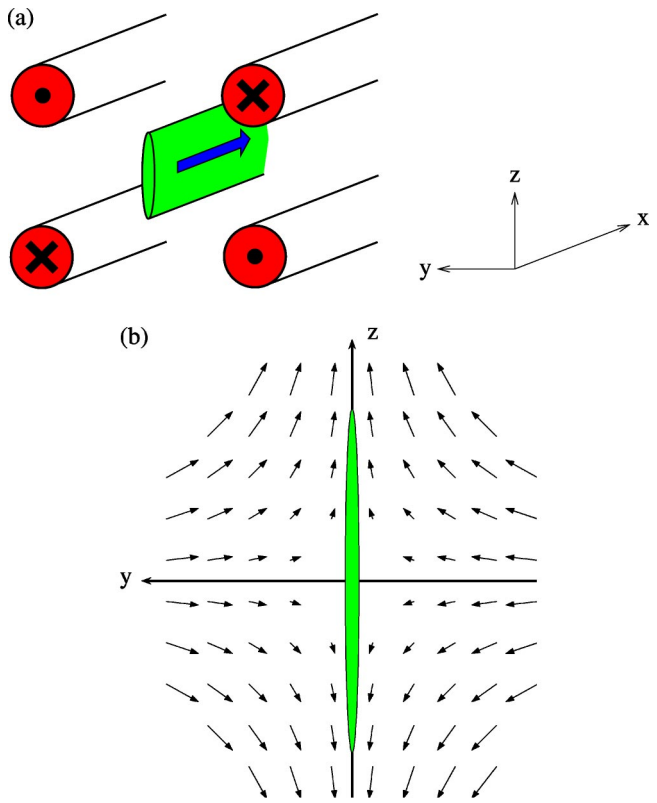

FIG. 1. (a) Cross section through an idealized set-up for a Stern-Gerlach measurement on an electron beam using a pulsed magnetic field. The shaped electron beam (shown as an ellipse with the arrow) passes between four wires which make a transient magnetic quadrupole field when a pulse of current flows (with directions indicated by • and ×). (b) The same section showing the detail of the field pattern around the wave packet. In both (a) and (b) the width of the wave packet is shown exaggerated.

position and momentum distribution determined by the initial quantum wave packet. The results of the classical simulation show good general agreement with the quantum results, in much the same way as there was general agreement between classical simulations and quantum results in Ref. [4].

In Sec. II A we first review the model system, which we have studied before and generalize it to time-dependent fields. The classical and quantum approaches to the problem will be described in Secs. II B and II C, respectively. A "scalar model" is introduced in Sec. II D, which provides information on the optimization of parameters in the quantum system. Then in Sec. III we present the main numerical results before concluding the paper in Sec. IV.

II. FRAMEWORK OF THE MODEL SYSTEM

This system, comprised of an electron and a time-dependent, spatially inhomogeneous magnetic field, can be described in several ways. In the following we look at model electromagnetic fields and a classical description of the electron. We then look at a quantum description of the system, and, finally, we consider a scalar model of the electron-field system, which gives insights into the best parameter choices for the quantum system.

A. The model electromagnetic fields

In order to consider the splitting of electron spin components in a time-dependent inhomogeneous magnetic field, we will use a simple model of the field. As well as being inhomogeneous in the direction of spin splitting, the field will have to be time dependent and preferably homogeneous in the direction of the electron beam (which we will take to be the x direction). The simplest form of inhomogeneous field we use is actually a magnetic quadrupole field with the vector potential

$$\mathbf{A}(\mathbf{r},t) = -a(t)yz\hat{\mathbf{x}}. \tag{1}$$

Note that we will use $\hat{\mathbf{x}},\hat{\mathbf{y}}$, and $\hat{\mathbf{z}}$ to represent the unit vectors in the x,y, and z directions, respectively. In Eq. (1) we have taken the coefficient a to be time dependent so that the field can be switched on and then switched off. The result of this time dependence is that during the transient period an electric field is also acting on the electron. From Eq. (1) the magnetic and electric fields are

$$\mathbf{B}(\mathbf{r},t) = \boldsymbol{\nabla} \times \mathbf{A} = a(t)(-y\hat{\mathbf{y}} + z\hat{\mathbf{z}}), \tag{2}$$

$$\mathbf{E}(\mathbf{r},t) = -\frac{\partial \mathbf{A}}{\partial t} = \frac{\partial a}{\partial t} yz\hat{\mathbf{x}}. \tag{3}$$

We wish to consider an electron which is initially free, but has a magnetic field of the form (2) switched on around it. A natural way of doing this is to use hyperbolic tangent functions to make a pulse of the form

$$a(t) = a_0\left[\tanh\left(\frac{t - t_c + t_p/2}{\tau}\right) - \tanh\left(\frac{t - t_c - t_p/2}{\tau}\right)\right] \Bigg/ \left[2\tanh\left(\frac{t_p}{2\tau}\right)\right] \tag{4}$$

as illustrated in Fig. 2, where a_0 is the peak value of the pulse at time $t=0$. The pulse width (at half height) is t_p, the center of the pulse is t_c, and the rise/fall time of the pulse is τ. The main emphasis in the following study will be on the effect of the steepness parameter τ, whose effect on the pulse shape can be seen in Fig. 2. In the following, the three cases shown will be utilized to monitor the effect of the switch on/off parameters.

B. Classical simulation

The classical forces on the electron arise from the Lorentz force and the dipole interaction (the coupling of the electron spin to the magnetic field). For the latter the potential energy of the electron magnetic moment in the field (2) is

$$U_S = -\boldsymbol{\mu} \cdot \mathbf{B}. \tag{5}$$

In the usual Stern-Gerlach device, a region of magnetic field is chosen for the beam so that B_z dominates; this results in a spin separation in the z direction. A simple offset along the z

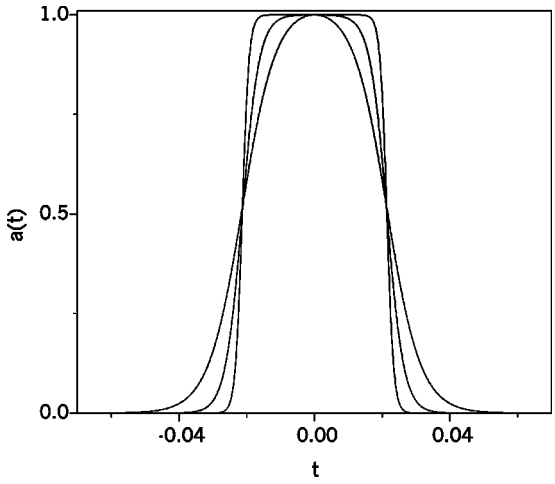

FIG. 2. The time-dependent magnetic-field gradient $a(t)$ as given by Eqs. (7) and (4) with $a_0=1$ and the pulse center at $t_c=0$. The rise times are $\tau=0.002\,52, 0.006\,30$, and 0.0126 with pulse width $t_p=0.0427$. The value of t_p is chosen to match the interaction time t_0 in Ref. [4]

axis ensures this. However, in past work [4] we have found that an input beam, or wave packet, is optimal for spin separation if it is much narrower in one transverse direction than the other. If we make an input wave packet narrow in the y direction compared to the z direction then it is also possible to get spin separation of z components because there is only a small portion of the electron wave packet in the low-field region, near the origin, where spin flips can obscure the result.

In classical simulations the input "wave packet" consists of an ensemble of classical particles with a Gaussian distribution corresponding to the quantum-mechanical probability distribution (in space and momentum). The magnetic dipole force on a classical electron from Eq. (5) can then be taken to be

$$F_z = \pm \mu\left(\frac{\partial B_z}{\partial z}\right) \tag{6}$$

with the sign depending on the spin component considered. For our model field the gradient is simply

$$\frac{\partial B_z}{\partial z} = a(t). \tag{7}$$

Then for classical simulations of the electron motion the resulting equation of motion (including both Lorentz forces and dipole forces) is

$$m\frac{d}{dt}\mathbf{v} = -e\mathbf{v}\times\mathbf{B}(\mathbf{r},t) - e\mathbf{E}(\mathbf{r},t) \pm \mu\left(\frac{\partial B_z}{\partial z}\right)\hat{\mathbf{z}}. \tag{8}$$

If we make use of Eqs. (2), (3), and (7) this may be written, for both spin components, as

$$m\frac{dv_x}{dt} = -ea(t)(v_y z + v_z y) - e\frac{\partial a}{\partial t}yz,$$

$$m\frac{dv_y}{dt} = ea(t)v_x z,$$

$$m\frac{dv_z}{dt} = a(t)(ev_x y \pm \mu). \tag{9}$$

Thus the numerical problem becomes that of integrating ordinary differential equations for each spin component over an ensemble of classical particles which represent the initial wave packet.

C. Quantum simulation

To perform quantum-mechanical simulations, we utilize the Hamiltonian for the spinor system with the potential energy (5) replaced by the expression

$$-\mu\boldsymbol{\sigma}\cdot\mathbf{B} = -\mu a\begin{bmatrix} z & iy \\ -iy & -z \end{bmatrix}, \tag{10}$$

where $\boldsymbol{\sigma}$ is comprised of the Pauli spin matrices ($\boldsymbol{\sigma}\equiv\sigma_x\hat{\mathbf{x}}+\sigma_y\hat{\mathbf{y}}+\sigma_z\hat{\mathbf{z}}$). Thus the total Hamiltonian is of the form

$$\begin{aligned} H_T &= \frac{(\mathbf{p}+e\mathbf{A})^2}{2m} - \mu\boldsymbol{\sigma}\cdot\mathbf{B} \\ &= \frac{p_x^2}{2m} + \frac{p_y^2}{2m} + \frac{p_z^2}{2m} - \frac{p_x}{m}eayz + \frac{(eayz)^2}{2m} - \mu\boldsymbol{\sigma}\cdot\mathbf{B}, \end{aligned} \tag{11}$$

where (in the second line) we have used the fact that our vector potential (1) only has a x component.

Inspection of the Hamiltonian shows that p_x is a conserved quantity (i.e., $[H_T,p_x]=0$). We note that, as is well known, this does not mean that v_x is constant. Given that the x direction is the direction of the electron beam, we can now consider that the spatial wave function in the x direction is a plane wave (monochromatic beam). That is, if the wave function Ψ can be expressed as

$$\Psi(x,y,z,t) = \psi(y,z,t)\exp\left(ik_x x - i\hbar\frac{k_x^2}{2m}t\right), \tag{12}$$

then $\psi(y,z,t)$ obeys the following Schrödinger equation:

$$i\hbar\frac{\partial\psi}{\partial t} = H\psi(y,z,t) \tag{13}$$

with

$$H = \frac{p_y^2}{2m} + \frac{p_z^2}{2m} - \frac{\hbar k_x}{m}eayz + \frac{(eayz)^2}{2m} - \mu\boldsymbol{\sigma}\cdot\mathbf{B}. \tag{14}$$

The original 3D problem has now been reduced to a 2D one which is easier to solve numerically.

The numerical integration of Eq. (13) is performed using a fast Fourier transform split-operator method [7] on a 2D grid of 512×512 points. We introduce a length scale l and a time scale τ such that (see Ref. [4])

$$l^3 = \frac{2\hbar}{ea_0}, \tag{15}$$

$$\tau = \frac{m}{\hbar} l^2, \tag{16}$$

where a_0 gives the maximum gradient of the magnetic field [see Eqs. (4) and (7)]. Then the Schrödinger equation (13) becomes

$$i\frac{\partial \psi}{\partial t} = \left\{ -\frac{1}{2}\left(\frac{\partial^2}{\partial y^2} + \frac{\partial^2}{\partial z^2} \right) - \Omega^2 f(t) yz + 2f(t)^2 y^2 z^2 - f(t) \times \begin{bmatrix} z & iy \\ -iy & -z \end{bmatrix} \right\} \psi \tag{17}$$

with $\Omega^2 = 2k_x l$ and the scaled field gradient $f(t) = a(t)/a_0$.

One advantage of the Fourier transform method of integrating Eq. (13), or Eq. (17), is that the image of the wave packet in momentum space is readily available. This can clearly show splitting of wave packet components even if the splitting is not yet manifest in physical space [4].

D. A scalar model

To carry out the integration of the Schrödinger equation (17), and to obtain a good spin separation, we need to select optimized parameters for the initial wave packet and the pulse. For the time independent case in Ref. [4] the choice of these parameters was informed by a *scalar model* of a slightly simplified quantum system. We can generalize that treatment here to the time-dependent case where we have the additional complication of free evolution of the initial wave packet before the pulse is switched on. That is, we need to find the optimal time t_c for the center of the pulse. The propagation of the wave packet is assumed to start at time zero, so for a large t_c we have a long free evolution, when a narrow wave packet can spread rapidly, while a very short time t_c means that the packet is prepared with the field already turned on as in the previous treatment.

The scalar model is defined by the Hamiltonian

$$H_{\pm} = \tfrac{1}{2}(p_y^2 + p_z^2) - \Omega^2 f(t) yz \pm f(t) z, \tag{18}$$

where we neglect the quadratic term in y and z and the off-diagonal terms of Eq. (17). With the new variables

$$\xi = \frac{1}{\sqrt{2}}(y+z),$$

$$\eta = \frac{1}{\sqrt{2}}(y-z), \tag{19}$$

the Hamiltonian takes the form

$$H = \left[\frac{1}{2}p_\xi^2 - \frac{\Omega^2 f(t)}{2}\left(\xi - \frac{\kappa}{\sqrt{2}\Omega^2} \right)^2 \right] + \left[\frac{1}{2}p_\eta^2 + \frac{\Omega^2 f(t)}{2}\left(\eta - \frac{\kappa}{\sqrt{2}\Omega^2} \right)^2 \right] \tag{20}$$

with $\kappa = \pm 1$. The solution for the Heisenberg equation of motion for the operators can be written in terms of functions $C_k(t)$, with $k = 1-4$, such that

$$\frac{\partial \hat{\xi}}{\partial t} = \hat{p}_\xi = \hat{p}_\xi^0 C_1'(t) + \Omega\left(\hat{\xi}^0 - \frac{\kappa}{\sqrt{2}\Omega^2} \right) C_2'(t),$$

$$\frac{\partial \hat{\eta}}{\partial t} = \hat{p}_\eta = \hat{p}_\eta^0 C_3'(t) + \Omega\left(\hat{\eta}^0 - \frac{\kappa}{\sqrt{2}\Omega^2} \right) C_4'(t). \tag{21}$$

Then the functions $C(t)$ should satisfy the equations

$$C_{1,2}'' = \Omega^2 f(t) C_{1,2}(t),$$

$$C_{3,4}''(t) = -\Omega^2 f(t) C_{3,4}(t), \tag{22}$$

with initial conditions $C_1(0) = C_3(0) = C_2'(0) = C_4'(0) = 0$, $C_1'(0) = C_3'(0) = 1$, and $C_2(0) = C_4(0) = 1/\Omega$. Using Eq. (21) we have for the momentum in the z direction

$$\hat{p}_z = \frac{1}{2}[\hat{p}_z^0 F_2(t) + \hat{p}_y^0 F_1(t)] + \frac{\Omega}{2}[\hat{z}^0 F_3(t) + \hat{y}^0 F_4(t)] - \frac{\kappa}{2\Omega} F_4(t), \tag{23}$$

where we have defined

$$F_1(t) = C_3'(t) - C_1'(t), \quad F_2(t) = C_3'(t) + C_1'(t),$$

$$F_3(t) = C_4'(t) + C_2'(t), \quad F_4(t) = C_4'(t) - C_2'(t). \tag{24}$$

The amount of momentum splitting is determined from the terms proportional to κ, which thus becomes

$$P_D = \frac{F_4(t)}{\Omega}. \tag{25}$$

We now define a resolution parameter as the dispersion of $\hat{p}_z$, $\sigma_z^2 = \langle (\hat{p}_z - \langle \hat{p}_z \rangle)^2 \rangle$, divided by the splitting

$$s^2(t) = \frac{\sigma_z^2}{P_D^2} = \frac{\Omega^2}{4}\left[\Delta p_y^2 \left(\frac{F_1(t)}{F_4(t)} \right)^2 + \Delta p_z^2 \left(\frac{F_2(t)}{F_4(t)} \right)^2 + \Omega^2 \Delta z^2 \left(\frac{F_3(t)}{F_4(t)} \right)^2 + \Omega^2 \Delta y^2 \right]. \tag{26}$$

Here we have introduced the initial widths $\Delta p_y^2 = \langle (\hat{p}_y^0)^2 \rangle$, etc.

In our time-dependent pulse model we want to minimize $s^2(t)$ in the limit $t \to \infty$. With initial minimum uncertainty wave packets, $\Delta p_y \Delta y = \Delta p_z \Delta z = 1/2$, we may optimize the resolution parameter independently with respect to y and z; see Ref. [4]. After minimizing with respect to the initial widths we obtain

$$s^2 = \frac{\Omega^3}{4}\left(\frac{F_1(\infty)F_4(\infty) + F_2(\infty)F_3(\infty)}{F_4(\infty)^2} \right). \tag{27}$$

Figure 3 shows the numerical calculation of s^2 (solid line) according to Eq. (27) as a function of t_c for the hyperbolic

tangent pulse with the intermediate slope in Fig. 2. This has been obtained by integrating the differential equations (22) to obtain the functionvalues in Eq. (24). The kink in the curve relates to the time $t_c \approx t_p/2$ when the pulse switches on at $t \approx 0$: i.e., before this time ($t_c < t_p/2$) the pulse is essentially on at the start of the time evolution ($t=0$), and after this time the pulse is essentially off.

The conclusion is clear: it is desirable to have the time t_c as short as possible consistent with the pulse being "off," i.e., as close to $t_p/2$ as possible in our model. We can gain considerable insight into the behavior of the resolution parameter by considering an analytically solvable square pulse model where

$$f(t) = \begin{cases} 0, & t \leqslant t_c - t_p/2 \\ 1, & t_c - t_p/2 < t < t_c + t_p/2 \\ 0, & t \geqslant t_c + t_p/2 \end{cases} \tag{28}$$

and we eventually find that the resolution becomes

$$s^2 = \begin{cases} \dfrac{\Omega^3}{4}\left[\dfrac{\sinh 2\Omega(t_c + t_p/2) - \sin 2\Omega(t_c + t_p/2)}{[\sinh \Omega(t_c + t_p/2) + \sin \Omega(t_c + t_p/2)]^2}\right] & t_c \leqslant t_p/2 \\ \Omega^3\left[\dfrac{\Omega(t_p - 2t_c)\cos 2\Omega t_p - \Omega(t_p - 2t_c)\cosh 2\Omega t_p + 2\sinh 2\Omega t_p - 2\sin 2\Omega t_p}{8(\sinh 2\Omega t_p + \sin 2\Omega t_p)^2}\right] & t_c \geqslant t_p/2. \end{cases} \tag{29}$$

For small interaction times t_p we may expand the above expressions to first order and obtain

$$s^2 = \begin{cases} \dfrac{\Omega^4 t_p}{12} + \dfrac{\Omega^4 t_c}{6}, & t_c \leqslant t_p/2 \\ \dfrac{\Omega^4 t_p}{24} + \dfrac{\Omega^4 t_c}{4}, & t_c \geqslant t_p/2. \end{cases} \tag{30}$$

This approximation to the analytical result for the square pulse is shown in Fig. 3 (dashed curve) and agrees well with the numerical solution given earlier (solid curve). Thus, it is clear that t_c should be chosen to be short in order to have a good resolution, so the optimal situation is when the free evolution of the wave packet is as small as possible. The limiting case, with the pulse off at the initial time, will be close to $t_c = t_p/2$, and at this point the analytical model predicts a resolution of $s^2 = \Omega^4 t_p/6$ which is identical to the result given previously in Ref. [4]. However, note that, first, if t_p is reduced, the reduction in s^2 will be less than in the time-independent model, and second, reduction of t_p and t_c together is not necessarily a good idea because of other considerations arising from the initial wave-packet shape which also depend on t_p [4]. For example, the angular width of the initial wave packet should be small to ensure that the spin separates in a specific direction. Thus in the results that follow next we take the parameters of Ref. [4] for our initial wave packets, and choose the time t_c so that the pulse will switch on as soon as possible, given the values of τ and t_p.

III. RESULTS

Figure 4 shows the momentum space distributions for different rise times τ (as chosen in Fig. 2). The figure shows the distributions at the end of the current pulse, i.e., when the magnetic field has died out and there are no significant forces on the electron. As discussed in the preceding section, many of the parameters for this figure have been taken from the time-independent field case which was optimized in Ref. [4]. We note that the momentum splitting in the z direction is more or less independent of the rise time τ. This result is confirmed by the momentum sections in Fig. 5 which are taken along the z axis in momentum space and show the splitting more clearly. A more significant effect than any change in the momentum space wave-packet splitting is a change in the shape of the wave packets for different values of the pulse turn-on time τ. As can be seen in Fig. 4, we find

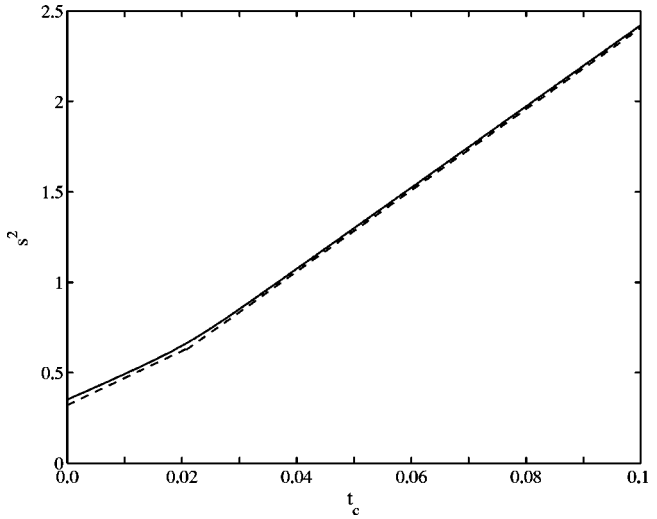

FIG. 3. The resolution s^2, Eq. (26), as a function of t_c. The solid line shows the numerical calculation of Eq. (27) for the pulse $\tau = 0.006\,30$ in Fig. 2. The dashed line is the result (30) for the square pulse.

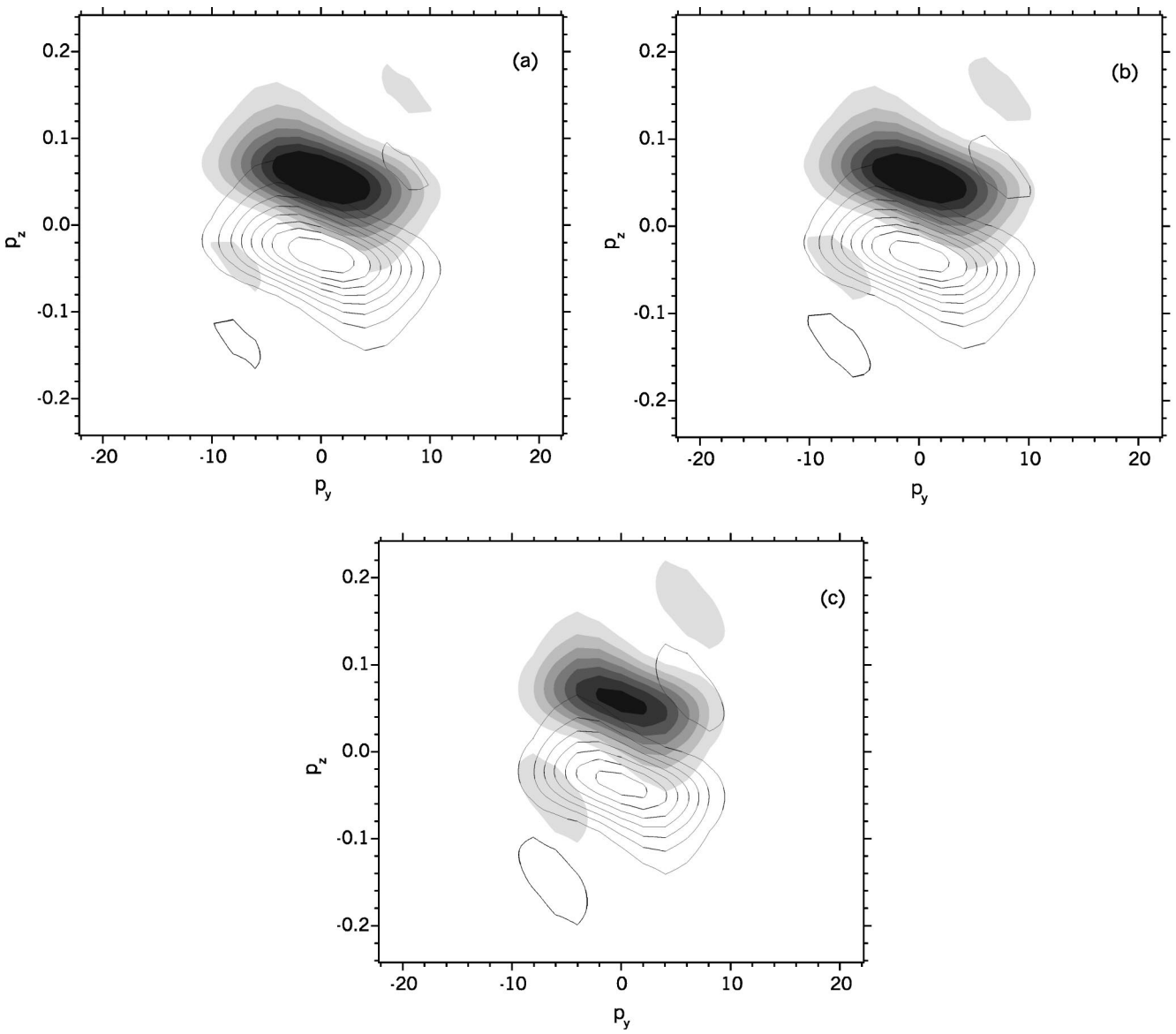

FIG. 4. Wave packets for the electron, in momentum space, shown after the field pulse. Parameters for the wave packet are (see Ref. [4]) $\Omega^2=9.48$, $\Delta y\sim 0.103$, and $\Delta z\sim 20.7$. The parameters for the pulse are $t_p=0.0427$, and (a) $\tau=0.002\,52$, $t_c=0.0302$; (b) $\tau=0.006\,30$, $t_c=0.0365$; and (c) $\tau=0.0126$, $t_c=0.0554$.

that increasing τ creates larger bumps in the wings of the wave packet, although $\tau=0.002\,52$ (a) and $\tau=0.006\,30$ (b) are very similar in Fig. 4. Such structure would make it more difficult to separate the two wave-packet components so it seems advantageous to have fast turn-on times.

The spatial pictures of the wave packets, corresponding to Fig. 5, do not show any discernible spatial splitting of the spin components at the time corresponding to Fig. 4. However, as we have pointed out previously [4], the splitting in momentum space is expected to manifest itself in real space given sufficient time. The spatial wave packets do change shape as τ increases; we find that there is more spreading in the y direction. Only one example is given in Fig. 6, since no spin splitting can be seen in coordinate space at this point in time.

An important issue relates to the fact that the electron beam turns in the magnetic (and electric) fields affecting it. In our previous work [4], we found that the forward electron velocity reduced considerably during the splitting process. Obviously this is undesirable since the normal functioning of a Stern-Gerlach device requires the beam to be traveling in a forward direction. However, forward motion after the interaction is guaranteed in a pulsed experiment such as the one we propose here. The reason is that the generalized momentum

$$p_x = mv_x + ea(t)yz \tag{31}$$

is conserved. This quantity is conserved both classically and quantum mechanically. Because the fields are switched off at the start and end of the experiment, $a(t=\pm\infty)\to 0$, the longitudinal electron velocity must be the same at the end of the

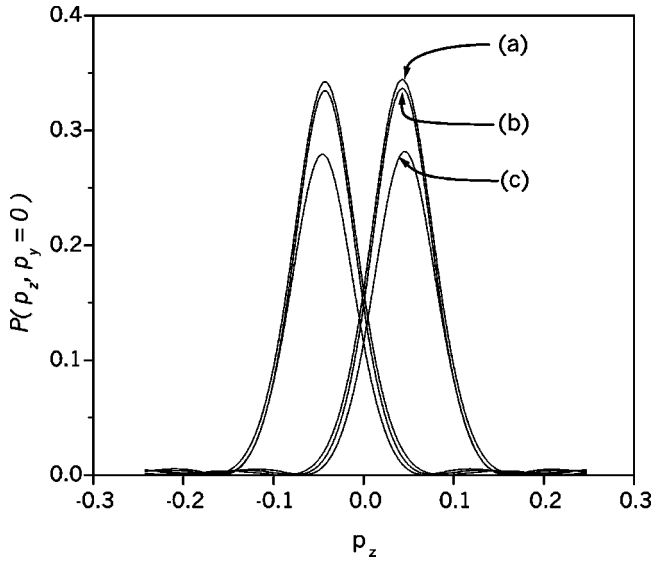

FIG. 5. Cross section at $p_y=0$ of the different momentum distributions for the same parameters as in Fig. 4.

field pulse as it was at the start. This is seen in Fig. 7 which shows the change in the forward velocity v_x as a function of time. The quantum curves can be computed from the wave packets using Eq. (31), since p_x is a constant and $\langle yz\rangle$ is easily found; see Ref. [4]. The slow reduction in electron velocity seen in Fig. 7 is followed by a sharp rise which is characteristic of the process. The slow fall is the response of the electron dynamics to the presence of the magnetic field. The sharp rise, on the time scale of the rise time τ, is the result of having to conserve p_x after v_x has fallen and $\langle xy\rangle$ increased. When $a(t)$ falls rapidly to zero, v_x must rise on the same time scale. The dashed lines in Fig. 7 also show the *classical* results for the forward velocity which have been computed from an ensemble of 20×10^6 electrons. The agreement is good at high velocities.

The ensemble number was chosen at 20×10^6 to ensure a reasonable accuracy from the classical simulations. This number was higher than expected and as a result the 3D classical simulations take longer to run on a computer than the integration of the time-dependent 2D Schrödinger equation. The reason for the high ensemble number required was

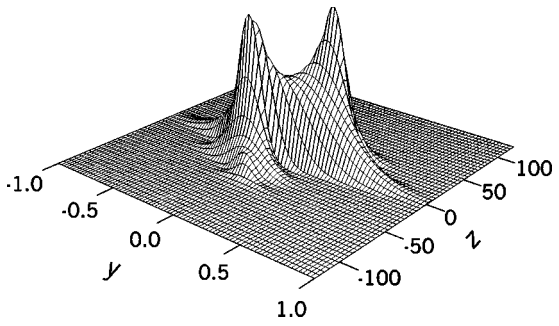

FIG. 6. Real space (rather than momentum space) picture of the wave packet shown in Fig. 4(a). The time, $t=0.061$, is after the field pulse, as is seen in Fig. 2 with $t_c=0.0302$ rather than $t_c=0$. At this time no spatial splitting of the spin components is yet seen.

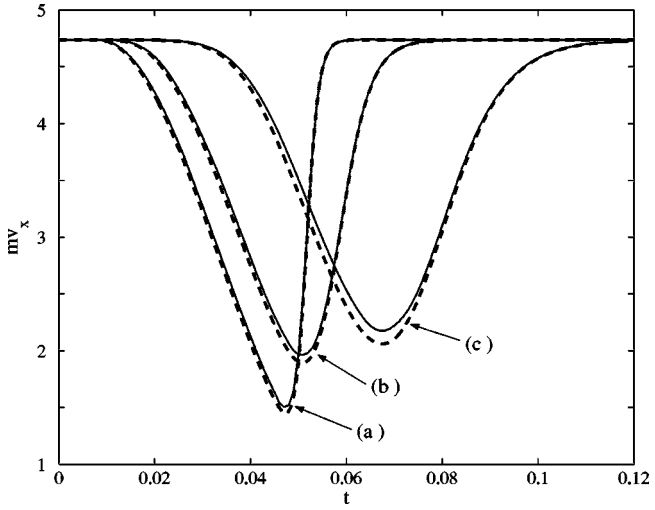

FIG. 7. Different forward velocities for the wave packet. Curves (a), (b), and (c) show the quantum-mechanical result with $\tau=0.002\,52$, $\tau=0.006\,30$, and $\tau=0.0126$, respectively. These and other parameters are as in Fig. 4. The dashed lines show the velocity from the corresponding classical simulations with 20×10^6 ensemble members.

that some of the final classical distributions have a Lorentzian character rather than (the original) Gaussian character. The relatively broad width of a Lorentzian function means that a larger ensemble is required for the same accuracy in the averages.

The beam quality is determined by the divergence angle which is proportional to $\langle p_z\rangle/mv_x$. When $v_x=\langle p_x\rangle/m$ is decreased the beam deteriorates, but this is compensated for when the fields are switched off. Then, however, the splitting in $\langle p_z\rangle$ emerges as the signature of the two spin components. In Fig. 8 we show the longitudinal velocity v_x, as a function of the splitting "signal" $\langle p_z\rangle$, with the interaction time parametrized. In effect this shows how the angle of divergence of the electron spin components develops. We see the gradual decrease of v_x, compare Fig. 7, followed by a rapid restoration of the forward velocity, as a function of $\langle p_z\rangle$, when the pulse switches off and the forward velocity is restored. When the interaction ceases, the curves show that the electron spin components end up with the maximum splitting achievable. These values are the average values of distributions such as those seen in Fig. 4. The angle of divergence of the electron spin components shows a very slight improvement in case (c) ($\tau=0.0126$) compared to the other cases presented, which have a shorter rise time τ. However, one should remember that as τ increases, the size of the secondary peaks (in momentum space) increase also (see Fig. 4). For clarity, in Fig. 8, we have only included the classical result for the case (b), which is represented by the dashed line in the figure. We note that the classical and quantum results for the momentum splitting actually agree quite well. However, we also note that a careful check of the widths of the wave packets shows that the width of the classical ensemble is broader than the width of the quantum wave packet, as found in Ref. [4]. Thus the quantum spin resolution is better than the classical spin resolution in this system.

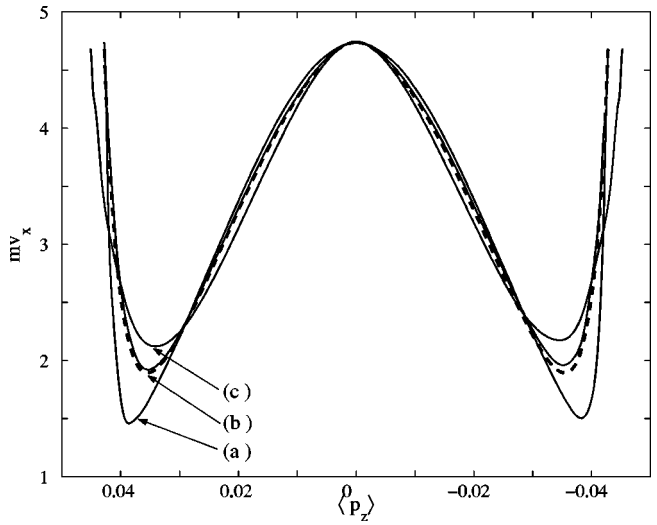

FIG. 8. Particle momentum in x and z directions for both spin components with time parametrized. Both components start at $\langle p_z\rangle=0$, but then move in opposite $\langle p_z\rangle$ directions as v_x falls and then rises. The final values indicate the diverging angle of the emerging electron beam spin components. The parameters for (a)–(c) are as in Fig. 4. The absolute values of the splitting in the three cases are (a) $\langle p_z\rangle=0.043$, (b) $\langle p_z\rangle=0.043$, and (c) $\langle p_z\rangle=0.045$. The dashed line is the result from a classical simulation with parameters as in curve (b) ($\tau=0.006\,30$) and 20×10^6 ensemble members.

IV. CONCLUSION

In this paper we have revisited the problem of an electron beam evolving in an inhomogeneous magnetic field, which we have studied by means of a 2D wave packet. The dynamics of the electron is complicated because of the combined effects of Lorentz and magnetic dipole forces which are of a similar size. This fact led Bohr to conclude that a separation of spin components would be impossible. However, in previous work we have shown that by manipulating the initial wave-packet shape a separation of spin components would just be possible. That argument required a free evolution of the wave packet after the interaction and the details of switching the field off were not considered until our work here. What we have found here is that a rapid switch off of the magnetic field is desirable and leads to a result of *just* separated components which is comparable to the previous work. In the limit of rapid pulse switching we can also apply our scalar model (with a square pulse) which can help optimize the parameters. Using this we found that it is not desirable, in the pulsed system, to let an initial Gaussian wave packet evolve before the field switches on. Thus the field should be switched on quickly, and as soon as the initial wave packet is prepared. The fact that the field later switches off is a big advantage in the pulsed model. This is because the forward velocity of electron beam is restored as the field goes off, leading to a better divergence of the spin components during the subsequent free evolution of the wave packets.

ACKNOWLEDGMENTS

We would like to acknowledge support from the Royal Swedish Academy of Sciences, the UK Engineering and Physical Sciences Research Council, and the European Union (under Contract No. HMPT-CT-2000-00096).

[1] B. M. Garraway and S. Stenholm, Contemp. Phys. **43**, 147 (2002).

[2] W. Pauli, in *Le Magnétisme*, Proceedings of the VI Solvay Conference, 1930 (Gauthier-Villars, Paris, 1932), Pt. II and discussion, pp. 217–280; reprinted in *Collected Scientific Papers by Wolfgang Pauli*, edited by R. Kronig and V. F. Weisskopf (Interscience, New York, 1964), Vol. 2, pp. 544–607.

[3] N. Bohr, *La Théorie Quantique des Champs* (Interscience, New York, 1962); reprinted in *Essays 1958-1962 on Atomic Physics and Human Knowledge* (Interscience, New York, 1963), p. 61.

[4] B. M. Garraway and S. Stenholm, Phys. Rev. A **60**, 63 (1999).

[5] G. A. Gallup, H. Batelaan, and T. J. Gay, Phys. Rev. Lett. **86**, 4508 (2001).

[6] H. Batelaan, T. J. Gay, and J. J. Schwendiman, Phys. Rev. Lett. **79**, 4517 (1997); G. H. Rutherford and R. Grobe, *ibid.* **81**, 4772 (1998); H. Batelaan and T. J. Gay, *ibid.* **81**, 4773 (1998).

[7] See, for example, B. M. Garraway and K.-A. Suominen, Rep. Prog. Phys. **58**, 365 (1995), and references therein.